ISSN 1674-1056
http://cpb.iphy.ac.cn
http://iopscience.iop.org/cpb
中国物理 B
Chinese Physics
中国物理 Chinese Physics B

A new technology for controlling *in-situ* oxygen fugacity in diamond anvil cells and measuring electrical conductivity of anhydrous olivine at high pressures and temperatures

Wen-Shu Shen(沈文舒)[1], Lei Wu(吴雷)[2], Tian-Ji Ou(欧天吉)[1], Dong-Hui Yue(岳冬辉)[1], Ting-Ting Ji(冀婷婷)[1], Yong-Hao Han(韩永昊)[1], Wen-Liang Xu(许文良)[3], Chun-Xiao Gao(高春晓)[1]

Citation: Chin. Phys. B . 2020, 29(1): 010702 . **doi:** 10.1088/1674-1056/ab5934
Journal homepage: http://cpb.iphy.ac.cn; http://iopscience.iop.org/cpb

What follows is a list of articles you may be interested in

Density functional theory investigation of carbon monoxide adsorption on the kaolinite (001) surface

Jian Zhao(赵健), Man-Chao He(何满潮), Xiang-Xing Hu(胡祥星), Wei Gao(高炜)
Chin. Phys. B . 2017, 26(7): 079101 . **doi:** 10.1088/1674-1056/26/7/079101

In-situ high pressure X-ray diffraction studies of orthoferrite $SmFeO_3$

Li Na-Na, Li Yan, Li Hui, Tang Rui-Lian, Zhao Yong-Sheng, Han Dan-Dan, Ma Yan-Mei, Cui Qi-Liang, Zhu Pin-Wen, Wang Xin
Chin. Phys. B . 2014, 23(6): 069101 . **doi:** 10.1088/1674-1056/23/6/069101

In-situ high-pressure behaviors of double-perovskite Sr_2ZnTeO_6

Han Dan-Dan, Gao Wei, Li Na-Na, Tang Rui-Lian, Li Hui, Ma Yan-Mei, Cui Qi-Liang, Zhu Pin-Wen, Wang Xin
Chin. Phys. B . 2013, 22(5): 059101 . **doi:** 10.1088/1674-1056/22/5/059101

A new technology for controlling *in-situ* oxygen fugacity in diamond anvil cells and measuring electrical conductivity of anhydrous olivine at high pressures and temperatures*

Wen-Shu Shen(沈文舒)[1], Lei Wu(吴雷)[2], Tian-Ji Ou(欧天吉)[1], Dong-Hui Yue(岳冬辉)[1], Ting-Ting Ji(冀婷婷)[1], Yong-Hao Han(韩永昊)[1], Wen-Liang Xu(许文良)[3], and Chun-Xiao Gao(高春晓)[1,†]

[1] *State Key Laboratory for Superhard Materials, Jilin University, Changchun* 130012, *China*
[2] *School of Mechatronics Engineering, Guizhou Minzu University, Guiyang* 550002, *China*
[3] *College of Earth Sciences, Jilin University, Changchun* 130061, *China*

(Received 30 September 2019; revised manuscript received 8 November 2019; accepted manuscript online 20 November 2019)

We present a novel technique for controlling oxygen fugacity, which is broadly used to *in-situ* measure the electrical conductivities in minerals and rocks during diamond anvil cell experiments. The electrical conductivities of olivine are determined under controlled oxygen fugacity conditions (Mo–MoO_2) at pressures up to 4.0 GPa and temperatures up to 873 K. The advantages of this new technique enable the measuring of the activation enthalpy, activation energy, and activation bulk volume in the Arrhenius relationship. This provides an improved understanding of the mechanism of conduction in olivine. Electrical conduction in olivine is best explained by small polaron movement, given the oxygen fugacity-dependent variations in conductivity.

Keywords: high pressure, high temperature, oxygen fugacity

PACS: 91.60.–x, 91.60.Gf, 91.60.Ki **DOI:** 10.1088/1674-1056/ab5934

1. Introduction

In-situ laboratory determinations of the electrical conductivities of minerals and rocks at high pressures and temperatures are the most robust and simple way to investigate the compositions, natures, and states of minerals in Earth's deep interior.[1,2] Such measurements are typically combined with magnetotelluric (MT) and geomagnetic deep sounding (GDS) to ascertain the mineral and chemical composition, thermodynamic state, presence, and distribution of water, and partial melting processes within the Earth.[3–10] Notably, the effect of oxygen fugacity on the electrical properties of a sample is far greater than those of temperature, pressure, and other factors in high temperature–pressure conductivity experiments.[11–13]

In conventional conductivity experiments, oxygen fugacity control can be achieved by manipulating the gas buffer proportions.[14] However, this method is only applicable to experimental devices at lower working pressures, such as piston cylinder presses.[15,16] Subsequently, a method of controlling oxygen fugacity with a solid oxygen buffer was used in high-pressure measurements. Xu *et al.*[17,18] proposed a new method of controlling the oxygen fugacity by using an Mo+MoO_2 (MMO) solid buffer in a multi-anvil apparatus, and successfully determined the electrical conductivity of (high-pressure) olivine. More recently, Dai *et al.*[19–23] used various solid buffers (*i.e.*, Fe_3O_4+Fe_2O_3, Ni+NiO, Fe+Fe_3O_4, Fe+FeO, Mo + MoO_2) on a YJ-3000t multi-anvil press to determine the conductivity of lherzolite, peridotite, and polycrystalline and hydrous olivine under controlled oxygen fugacity condition. Although the use of sintered diamond as a secondary anvil can attain lower mantle pressure condition ($\sim$ 80 GPa; $\leq$ 2000 K),[24,25] most multi-anvil apparatus are suitable for being used under condition of the upper mantle ($\sim$ 28 GPa; $\leq$ 2500 K).[26] Hence, diamond anvil cells (DAC) are used to attain high pressures that reach core–mantle boundary conditions.[27] Furthermore, very high temperatures ($\leq$ 4000 K) can be obtained with a DAC equipped with a laser heating system (LH-DAC). Combined with other experimental methods, the DAC set-up is used to mimic the temperature–pressure conditions of Earth's interior and measure the physical properties of typical mantle minerals.[28–31]

However, conductivity testing with a DAC may introduce relatively large systematic errors as a result of the following three factors. (i) The sample chamber is only hundreds of microns in size and the oxygen fugacity control method used in conventional multi-anvil press experiments is not suitable. As such, previous DAC mineral conductivity experiments have rarely considered the effects of oxygen fugacity.[32,33] (ii) Uncertainties exist in the sample thickness. Deformation of diamond and sealing gaskets make it difficult to measure the thickness of the sample. (iii) Electrical conductivity in a DAC experiment is typically measured by placing a thin metal wire electrode in the sample chamber,[34] but the shape and position

*Project supported by the National Natural Science Foundation of China (Grant Nos. 11674404, 41330206, and 11374121).
†Corresponding author. E-mail: cc060109@qq.com
© 2020 Chinese Physical Society and IOP Publishing Ltd

of the electrode wires cannot be fixed during pressure loading.

Given these limitations and inspired by the successful oxygen fugacity control in large-volume multi-anvil experiments, we have developed and presented a novel technique to control the oxygen fugacity in DAC experiments and conduct the completely accurate conductivity measurements. We use magnetron sputtering and thin-film micro processing technology to facilitate *in situ* oxygen fugacity control at high pressures and temperatures. Using this approach, we measure the conductivity of anhydrous olivine and compare the result with those previously measured. Our new technique is broadly applicable to conductivity measurements under high pressure andtemperature conditions of the deep Earth.

2. Materials and methods

2.1. Sample preparation

The olivine samples were obtained from the Damaping area of Hebei Province, China. The olivine was handpicked and then ground into powder in agate. Then, the powder samples were baked in a 393-K baking oven for 24 h to completely eliminate the adsorbed water in the whole assemblage. The chemical composition of the sample was determined by energy dispersive spectrometry (Fig. A1 in Appendix A) and is listed in Table 1. Subsequently, Fourier-transform infrared spectroscopy (FTIR) was used to verify the anhydrous nature of the sample prior to the conductivity measurements. The FTIR spectrum of olivine is shown in Fig. A2 (in Appendix A). The olivine water content was < 1 ppm, which we refer to as "anhydrous" olivine.

Table 1. Major chemical compositions of olivine material.

Composition	SiO_2	Al_2O_3	FeO	MgO	CaO	Na_2O	K_2O	Total
Content/wt%	40.26	0.75	3.99	54.68	0.21	0.02	0.09	99.81

2.2. Experimental method

The experiments under high pressures and temperatures were performed with the new DAC device as shown in Fig. 1(a). Two ceramic resistance-heating rings were used in the DAC. One was located inside the groove of the plate seat, and the other was located on the platform of the spherical seat. An external water cooling system was introduced to avoid pressure loss caused by heated DAC. The DAC was placed inside a vacuum chamber during the measurement. Figure 1(b) is the schematic diagram of the vacuum device. This vacuum system effectively suppresses the oxidation of the diamond anvil, and improves the temperature range of the experiment. At the same time, the vacuum environment minimizes the effect of thermal exchange and thermal convection of air, improves the effective utilization of heat, and reduces temperature measurement error. High pressure was generated by using a DAC with a 400-μm-diameter anvil culet. Pressure was measured by the ruby fluorescence method. No pressure-transmitting medium was used to avoid an additional error from the electrical measurements.

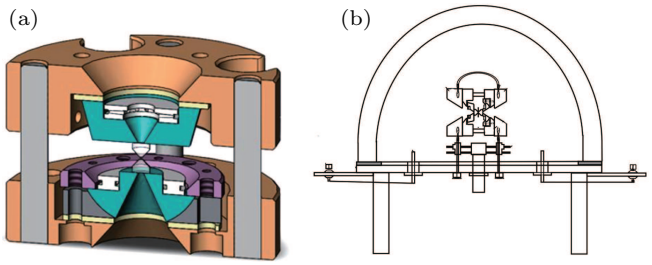


Fig. 1. (a) Section view of high pressure/high temperature DAC, and (b) schematic diagram of vacuum device.

To fabricate the microcircuit on the diamond anvil, we adapted the Gao *et al.*'s method[35] A mixed film of Mo and MoO_2 was sputtered on the face of the diamond anvil to form electrodes. The sputtering power was 90 W and the chamber working gas pressure was 1.0 Pa. The flow ratio of Ar to O_2 was 1.6 : 30. The film was then integrated into a two-electrode configuration microcircuit through photolithography. After the preparation of the electrical circuit, an alumina layer (Al_2O_3) was deposited on the circuit. This acted as an electrical and heat insulator and surrounded the microcircuit. A detection window was made in the center of the culet by removing the covering alumina, which kept the film electrode contacting the sample. The anvil and electrode configuration are shown in Figs. 2(a) and 2(b).

We developed a complex gasket, which is a metal gasket with an oxygen fugacity buffering ring and insulating gasket material as shown in Fig. 2(c). An Re tablet was used as the gasket. The gasket was pre-indented to 50 μm in depth. A hole with a diameter of 250 μm was drilled into the middle of the indentation. High-purity Mo and MoO_2 powders were packed into the hole and mixed uniformly according to the weight rate given from buffering equilibrium equation (*i.e.*, 86-wt% Mo+14-wt% MoO_2). After being firmly pressed, a new hole that is 150 μm in diameter was obtained in the center of the mixed powder. This cylinder of mixed Mo and MoO_2 powder forms a sealed atmospheric environment that controls the partial oxygen pressure in the sample chamber. In order to insulate the gasket from the electrodes on the anvils, BN powder was placed in the hole and compacted into a hole-shaped piece, which a smaller hole with 100 μm in diameter was then drilled into, resulting in a sample chamber. Figure 2(c) shows a cross-sectional view of the DAC. After measuring the electrical conductivity, the buffer was analyzed by x-ray diffraction (Fig. 3) to check whether Mo and MoO_2 are existent, and the results show that the oxygen fugacity in the sample chamber was fully controlled. We used Pt as a test electrode for a comparative experiment without oxygen fugacity control. Figures 2(d) and 2(f) show a photograph and schematic of the anvil with a Pt electrode, respectively.

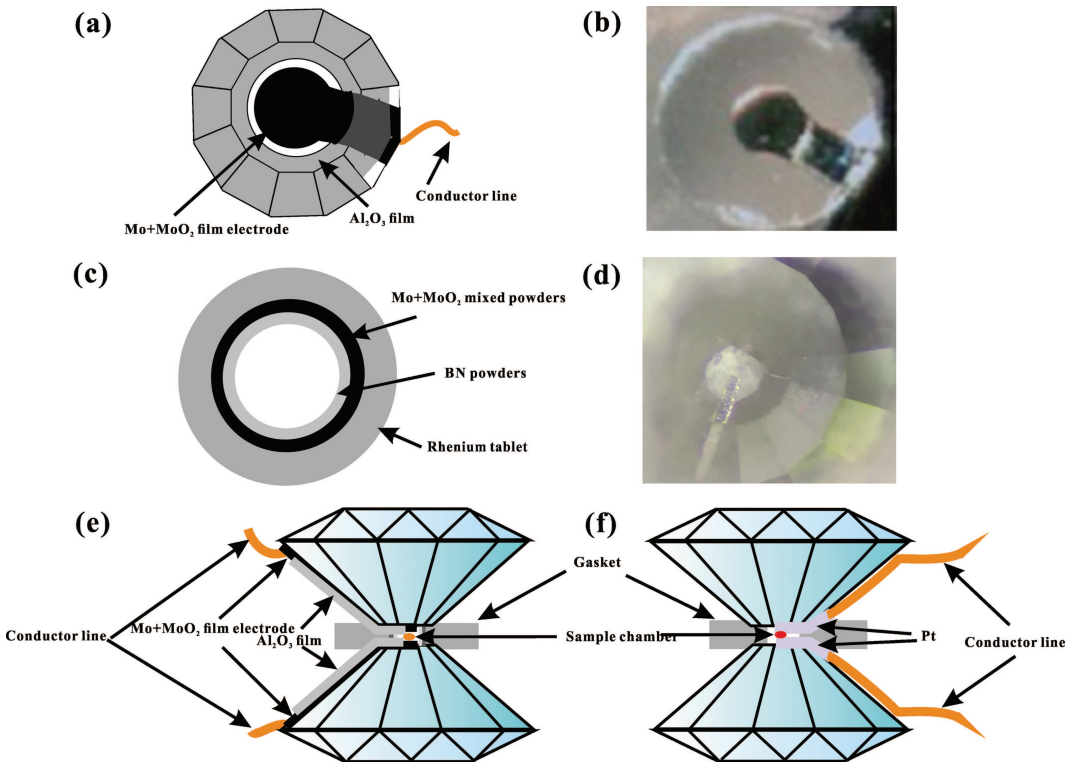


Fig. 2. (a) Schematic diagram of film microcircuit on diamond anvil cell, (b) photograph of electrode corresponding to panel (a), (c) configuration of composite insulating gasket, (d) photograph of Pt electrode, (e) cross-section of DAC showing Mo + MoO_2 film electrode, and (f) cross-section of DAC showing Pt electrode.

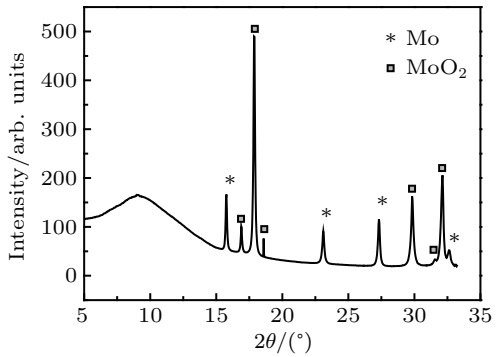


Fig. 3. X-ray diffraction pattern confirming Mo and MoO_2 buffer existing after conductivity has been measured.

A Solartron-1260 impedance/gain-phase analyzer was used to record the impedance spectrum. This was operated with a signal voltage of 1 V at frequency ranging from 10^{-1} Hz to 10^7 Hz. Temperature was varied in steps of 50 K, with the electrical conductivity being measured at each step. For the sample thickness measurements it was assumed that the diamond deformation was elastic and so was it during loading and unloading. If the gasket undergoes entirely plastic deformation, then the thickness of the sample (t) at each pressure during compression is

$$t = L_{\mathrm{m}} + \delta_{\mathrm{P}}, \tag{1}$$

where L_{m} is the sample thickness at maximum pressure and δ_{P} is the difference in thickness between loading and unloading for each pressure.[36,37]

3. Experimental results

In-situ measurements of the complex impedance of olivine are carried out at 1.0 GPa–4.0 GPa and 573 K–873 K. Figures 4(a) and (b) show the complex impedance curves of olivine obtained with Pt and Mo–MoO_2 electrodes, respectively. In Fig. 4(a), it is evident that the impedance arc diameter and impedance decrease markedly with temperature increasing and, as such, the electrical conductivity increases. The temperature dependence of the impedance arc diameter with the Mo–MoO_2 electrode is similar to that with the Pt electrodes, apart from the size of the change. We find that the resistance of olivine measured with the Mo–MoO_2 film electrodes is significantly smaller than that measured with Pt electrodes. The grain interior resistance is determined from a model of the electrical response, with the equivalent circuit of resistance (R) and a non-ideal constant-phase element (CPE). The equivalent circuit is shown in the inset in Fig. 4. Given that the contributions from the electrodes and grain boundaries are small, the olivine conductivity can be determined as follows:

$$\sigma = L/RS, \tag{2}$$

where L is the thickness of the sample (in unit m), S is the sample cross-sectional area (in unit m^2), and R is the measured resistance (in unit Ω).

At pressures in a range of 1.0 GPa–4.0 GPa and temperatures in range of 573 K–873 K, the relationship between

olivine conductivity and reciprocal temperature conforms to the Arrhenius equation:

$$\sigma = \sigma_0 \times \exp(-\Delta H/\kappa T), \tag{3}$$

where σ_0 is the pre-exponential factor (in units S/m), ΔH is the activation enthalpy, T is the temperature, and κ is the Boltzmann's constant. The relationship among activation enthalpy (ΔH), activation energy (ΔU; in unit eV), pressure (P; in unit GPa), and activation bulk volume (ΔV; in unit cm^3/mol) is

$$\Delta H = \Delta U + P\Delta V. \tag{4}$$

The relationship between electrical conductivity and temperature at 1.0 GPa–4.0 GPa is shown in Fig. 5. Table 2 details the activation enthalpy, energy, and volume calculated from Eqs. (7) and (4).

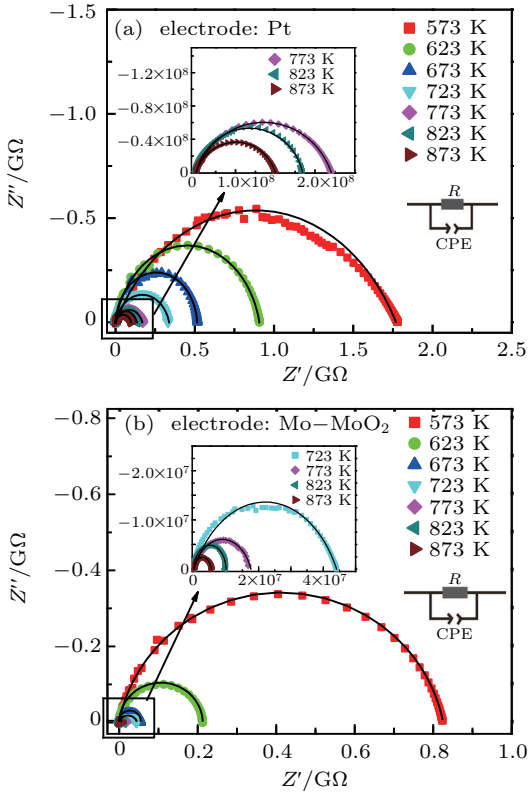


Fig. 4. Impedance spectra of olivine measured with (a) Pt electrodes and (b) Mo+MoO_2 film electrodes.

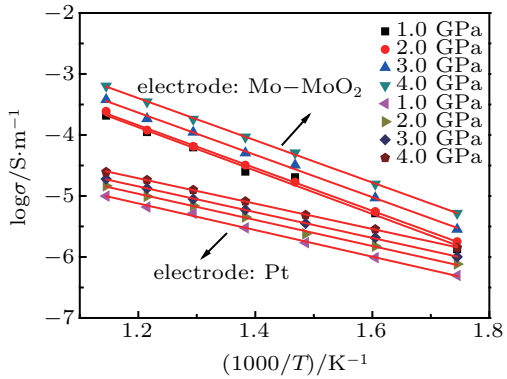


Fig. 5. Plots of $\log\sigma$ *versus* $1/T$ for olivine conductivity experiments with Pt and Mo+MoO_2 film electrodes at various pressures.

Table 2. Fitted parameter results for electrical conductivity of olivine.

Oxygen buffer	P/GPa	T/K	ΔH/eV	ΔU/eV	ΔV/m^3·mol^{-1}
No	1.0	573–873	0.432	0.438	–0.0069
No	2.0	573–873	0.424		
No	3.0	573–873	0.418		
No	4.0	573–873	0.411		
MMO	1.0	573–873	0.704	0.708	–0.0065
MMO	2.0	573–873	0.694		
MMO	3.0	573–873	0.686		
MMO	4.0	573–873	0.685		

4. Discussion

4.1. Conduction mechanism in olivine

Electrical conductivity increases with temperature increasing (Fig. 5). As is the case for dielectric medium isolators, the olivine charge carriers move by thermally excited hopping during conduction.[38,39] With the increase of temperature, the carriers have higher energy and more carriers can cross the energy barrier. Electrical conductivity and carrier concentration are linked by the relationship described by the Nernst–Einstein equation

$$\sigma = nq\mu, \tag{5}$$

where σ is the conductivity, n is the charge carrier concentration, and q is the effective charge. Therefore, an increase in the carrier concentration leads to a higher sample conductivity.

A monotonic linear relationship exists between the logarithm of electrical conductivity and temperature, which suggests that only one olivine conduction mechanism exists at 573 K–873 K. The main mantle minerals (*i.e.*, ferromagnesian silicates) typically have three conduction mechanisms, *i.e.*, protons, small polarons, and ions.[40] Different conduction mechanisms can be distinguished from the activation enthalpy and activation bulk volume.[10,41,42] The activation enthalpy of the proton conduction mechanism in hydrous silicate is typicall $y < 1.0$ eV and is weakly dependent on temperature. The activation enthalpy and activation bulk volume in our experiments are relatively low ($\Delta H < 1.0$ eV; Table 2); however, the FTIR spectra of our olivine sample show that it is essentially anhydrous, in addition, the measured electrical conductivity is strongly dependent on temperature. Moreover, the experimental temperature is not high enough to generate protons, meaning that the proton conduction is implausible. The ion conduction mechanism is not viable either, given that the activation energy for this mechanism is generally more than 2.0 eV.[43] This mechanism would also only be likely to occur for experimental temperatures of > 1500 K. Therefore, small polarons are likely the main charge carriers in our experiments. The activation volumes (ΔV) are negative (Table 2), which supports the suggestion that olivine experienced small polaron hopping conduction. This conduction mechanism refers to the directional hopping of a bound hole along

a directional electrical field. In our experiment, the activation enthalpy decreases with pressure increasing. A decrease in the average Fe^{3+}–Fe^{2+} distance by compression facilitates electron hole hopping between Fe^{3+} and Fe^{2+}. Thus, the activation enthalpy decreases with pressure increasing. It is also strong evidence of a small polaron conduction mechanism in our experiments.

The conductivities of olivine measured without oxygen fugacity buffering are clearly lower than those measured with buffering (Fig. 5). The Mo + MoO_2 film electrode provides a better oxygen atmosphere than when using a Pt electrode. According to the point defect oxidation–reduction reaction,[39] the point defect reactions between O in the sample chamber and Fe^{2+} in the sample occur under certain temperature conditions. As such, the Fe^{2+} that occupies the Mg^{2+} site in the olivine structure is oxidized into a small polaron. Consequently, the electron (e') and hole ($h^{\bullet}$) are of the main defect types. With time going by, concentrations of Fe^{X}_{Mg} and $Fe^{\bullet}_{Mg}$ reach a buffered equilibrium. The small polaron conduction in olivine takes place by polaron hopping between holes in the lattice Fe^{2+} sites, and can be expressed as

$$O^{X}_{O} = \frac{1}{2}O_2 + V^{\bullet\bullet}_{O} + 2e', \tag{6}$$

$$Fe^{X}_{Mg} + h^{\bullet} = Fe^{X}_{Mg}, \tag{7}$$

where O^{X}_{O} is the oxygen ion, O_2 is the oxygen in the sample chamber, $V^{\bullet\bullet}_{O}$ is the oxygen vacancy, e' is the electron, Fe^{X}_{Mg} is the Fe^{2+} occupying the Mg^{2+} site in the lattice structure of the sample, $h^{\bullet}$ is the hole, and $Fe^{\bullet}_{Mg}$ is the Fe^{3+} in the lattice Mg^{2+} site. The increase in oxygen fugacity leads to higher small polaron concentrations produced by point defect reactions, which increases the electrical conductivity. As is well known, iron in the sample will be lost to the Pt measuring electrode during the experiment,[44] resulting in a decrease in carrier concentration and a decrease in the conductivity of olivine. Therefore, the conductivity values obtained with an oxygen fugacity buffer are higher than those measured without a buffer.

4.2. Comparison with previous research

We compare our olivine conductivity data with the data from previous studies.[18,22,45,46] The data obtained with an oxygen fugacity buffer are in better agreement with previous experiments than with those determined without a buffer (Fig. 6). The activation enthalpies (0.685 eV–0.704 eV) of olivine measured with oxygen fugacity buffers are similar to those published by Yoshino *et al.* and Sakamoto *et al.*, *i.e.*, 0.74 eV–0.98 eV for the low-temperature region and 0.29 eV–0.67 eV, respectively. However, activation enthalpies (0.411 eV–0.432 eV) determined for olivine without an oxygen fugacity buffer are obviously lower than those of all previous studies. The Fe content ($X_{Fe} = Fe/(Fe+Mg) = 0.18$) of olivine in our experiments is close to that of Yoshino *et al.* ($X_{Fe} = 0.2$). If we extrapolate the olivine conductivity to $T > 873$ K, then the conductivity obtained with an oxygen fugacity buffer is comparable to that reported by Yoshino *et al.* Their difference in Fe content, mineralogical composition, and redox condition of olivine show that our obtained conductivity value is than that reported by Sakamoto *et al.* The activation enthalpy of olivine measured with an oxygen fugacity buffer is lower than the values reported by Dai *et al.* and Xu *et al.*, *i.e.*, 143.77 kJ/mol–151.44 kJ/mol and 1.40 ± 0.5 eV, respectively, which we attribute to the different temperature conditions and mineralogical compositions used in the various studies. In summary, our values obtained with oxygen fugacity buffering are close to those of previous studies, but the results determined without buffering are discrepant. Therefore, the conductivity data obtained by using our oxygen fugacity control technique during DAC experiments are robust and as reliable as the data obtained in multi-anvil experiments.

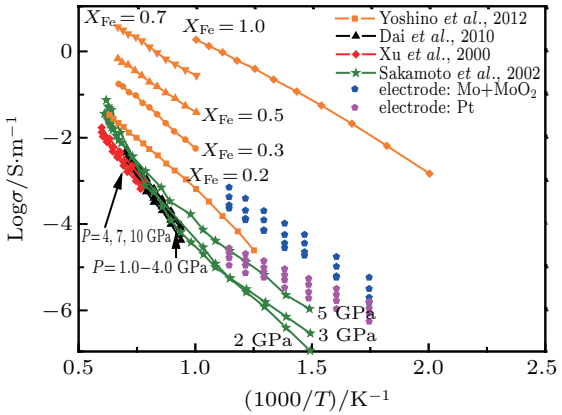


Fig. 6. Comparison of our olivine electrical conductivity measurements with previous studies.

5. Conclusions

We present a novel technique for controlling the oxygen fugacity during DAC experiments, which combines magnetron sputtering and thin film photolithography technologies. Oxygen fugacity buffering rings in a composite insulating gasket composed of Mo and MoO_2 form a closed sample chamber that can control the oxygen atmosphere. The Mo and MoO_2 on the diamond anvil surface not only provide an oxygen atmosphere for the sample, but also serve as an electrode for measuring the electrical properties of a sample at high temperature and pressure. This new technique solved the problem of the previous lack of oxygen fugacity control in DAC experiments.

We determine the olivine conductivity parameters with our new method at 523 K–873 K and 1.0 GPa–4.0 GPa. With temperature increasing, the electrical conductivity increases, according to the Arrhenius relationship. The measured olivine conductivity parameters indicate that the dominant conduction mechanism is by small polarons. Our results show that

the sample oxidation conditions are well buffered by the Mo–MoO_2 reaction. This new technique can reduce uncertainties compared with conventional DAC experiments, due to careful consideration of the sample environment, including ensuring temperature homogeneity, correcting sample thickness, and eliminating current leakage by using an insulating gasket. This new method can be used to accurately measure the mineral and rock conductivity in the deep Earth, and can also be applied to other experiments where oxygen fugacity control is desirable.

Appendix A: Supporting information

A1. The chemical compositions of olivine by energy dispersive spectroscopy (EDS)

The energy dispersive spectrum analysis of olivine is shown in Fig. A1, revealing the presence of Si, Mg, Ca, Fe, Al, K, Na, and O.

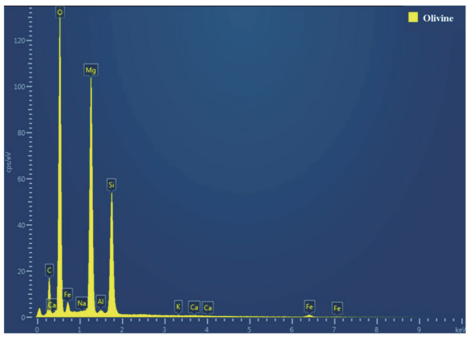


Fig. A1. Energy dispersive spectrum of olivine.

A2. Determuning the water content of the sample

We use the Paterson calibration to determine the water content of the sample

$$C_{\mathrm{W}} = \frac{B_{\mathrm{j}}}{150\xi}\int \frac{K(\nu)}{(3780-\nu)}\mathrm{d}\nu,$$

where C_{W} is the molar concentration of hydroxyl (ppm wt H_2O or H/10^6 Si), B_{j} is the density factor (4.39×10^4 cm H/10^6 Si), ξ is the orientation factor (1/3), and $K(\nu)$ is the absorption coefficient in unit cm^{-1} at wavenumber ν in unit cm^{-1}. The integration is conducted from 3000 cm^{-1} to 3750 cm^{-1}.

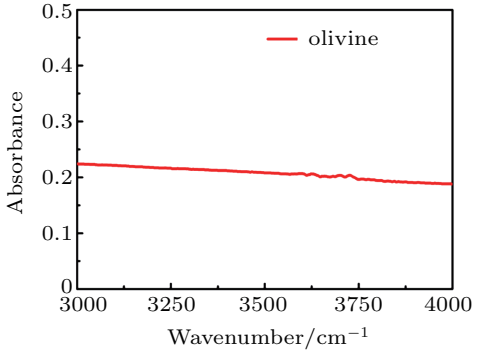


Fig. A2. FTIR spectrum of olivine.

References

[1] Ohta K, Hirose K and Ichiki M 2010 *Earth Planet. Sci. Lett.* **289** 497
[2] Poe B T, Romano C, Nestola F and Smyth J R 2010 *Phys. Earth Planet. Inter.* **181** 103
[3] Duba A, Heikamp S, Meurer W, Nover G and Will G 1994 *Nature* **367** 59
[4] Gailland F, Malki M, Lacono-Marziano G, Pichavant M and Scaillet B 2008 *Science* **322** 1363
[5] Glover P W J and Vine F J 1992 *Nature* **360** 723
[6] Manthilake G, Mookherjee M, Bolfan-Casanova N and Andrault D 2015 *Geophys. Res. Lett.* **42** 7398
[7] Reynard B, Mibe K and Van de Moortele B 2011 *Earth Planet. Sci. Lett.* **307** 387
[8] Wang D, Guo Y, Yu Y and Karato S I 2012 *Contrib. Mineral. Petr.* **164** 17
[9] Yang X 2012 *Earth Planet. Sci. Lett.* **317–318** 241
[10] Yoshino T 2010 *Surv. Geophys.* **31** 163
[11] Du Frane W L, Roberts J J, Toffelmier D A and Tyburczy J A 2005 *Geophys. Res. Lett.* **32** L24315
[12] Schock R N, Duba A G, Heard H C and Stromberg H D 1977 in *High Pressure Res.: Appl. Geophys*, edited by Manghnani M and Akimoto S (New York: Academic Press) pp. 39–51
[13] Wood B J and Nell J 1991 *Nature* **351** 309
[14] Duba A and Nicholls I A 1973 *Earth Planet. Sci. Lett.* **18** 59
[15] Seifert K F, Cemic L, Hinze E, Voight R and Will G 1980 *High Pressure Science and Technology* (Oxford: Pergamon Press) pp. 884–890
[16] Seifert K F, Will G and Voigt R 1982 *High-Pressure Researches in Geoscience* (Stuttgart: E Schweizerbart'sche Verlagsbuchhandlung) pp. 419–432
[17] Xu Y S, Poe B T, Shankland T J and Rubie D C 1998 *Science* **280** 1415
[18] Xu Y S, Shankland T J and Duba A G 2000 *Phys. Earth Planet. Inter.* **118** 149
[19] Dai L D and Karato S I 2014 *Phys. Earth Planet. Inter.* **232** 57
[20] Dai L D, *et al.* 2008 *J. Phys. Chem. Solids.* **69** 101
[21] Dai L D, Li H, Hu H and Shan S 2008 *J. Geophys. Res.* **113**
[22] Dai L D, Li H, Li C, Hu H and Shan S 2010 *Mineralogical Magazine* **74** 849
[23] Dai L D, Li H, Hu H and Shan S 2011 *Chin. Phys. B* **20** 049101
[24] Tange Y, Irifune T and Funakoshi K 2008 *High Press. Res.* **28** 245
[25] Tange Y, Takahashi E, Nishihara Y, Funakoshi K I and Sata N 2009 *J. Geophys. Res.* **114** B02214
[26] Xie H S 1977 *An introduction to Earth's deep material science* (Beijing: Science Press) pp. 1–228
[27] Bassett W 2009 *High Press. Res.* **29** 163
[28] Hu Q Y, *et al.* 2016 *Nature* **534** 241
[29] Hu Q Y, *et al.* 2017 *Proc. Natl. Acad. Sci. USA* **114** 1498
[30] Mao Z, Lin J, Liu J, Alatas A, Gao L, Zhao J and Mao H K 2012 *Proc. Natl. Acad. Sci. USA* **109** 10239
[31] Zhang L, *et al.* 2014 *Science* **344** 877
[32] Ohta K, Hirose K, Lay T, Sata N and Ohishi Y 2008 *Earth Planet. Sci. Lett.* **267** 107
[33] Ohta K, *et al.* 2008 *Science* **320** 89
[34] Ohta K, Hirose K, Onoda S and Shimizu K 2007 *Proc. Jpn. Acad. Ser. B* **83** 97
[35] Han Y H, *et al.* 2005 *Appl. Phys. Lett.* **86** 064104
[36] Li M, *et al.* 2007 *Appl. Phys. Lett.* **90** 113507
[37] Li M, *et al.* 2007 *Rev. Sci. Instrum.* **78** 075106
[38] Hirsch L M and Shankland T J 1993 *Geophys. J. Int.* **114** 21
[39] Wanamaker B J 1994 *Geophys. Res. Lett.* **21** 21
[40] Katsura T, Yoshino T, Manthilake G and Matsuzaki T 2009 *Russ. Geol. Geophys.* **50** 1139
[41] Yoshini T, Laumonier M, McIsaac F and Katsura T 2010 *Earth Planet. Sci. Lett.* **295** 593
[42] Goddat A, Peyronneau J and Poirier J P 1999 *Phys. Chem. Miner.* **27** 81
[43] Katsura T, Sato K and Ito E 1998 *Nature* **395** 493
[44] Wanamaker B J and Duba A G 1993 *J. Geophys. Res.* **98** 489
[45] Yoshino T, Akira S, Shuanming Shan, Guo X Z, Daisuke Y, Eiji I, Yuji H and Ken-ichi F 2012 *J. Geophys. Res.* **117** B08205
[46] Sakamoto D, *et al.* 2002 *J. Phys.: Condens. Matter* **14** 11375